https://adv-j-sci-eng.com eISSN: 2717-0705

Advanced Journal of Science and Engineering

Original Research

Friction Stir Welding of CuZn40 Brass Alloy based on Optimal Response Surface Results: Numerical and Experimental Analyses

Afshin Emamikhah[1,✉], **Amir Jamali**[2], **Afshin Kazerooni**[1], **Amir Mehdikhani Soleimanloo**[1]

[1] *Department of Mechanical Engineering, Shahid Rajaee Teacher Training University, Tehran, Iran*

[2] *Department of Materials and Metallurgical Engineering, Amirkabir University of Technology, Tehran, Iran*

✉ *Corresponding author*: **A. Emamikhah**; *E-mail address*: **afshin.emamikhah@gmail.com**, *ORCiD*: **0000-0001-6976-0057**.

Received: 18 October 2020 / ***Accepted***: 19 November 2020 / ***Published Online***: 30 March 2021

ABSTRACT

CuZn40 brass alloy with 38-42% zinc content has different applications regarding its formability and machinability properties. In this study, friction stir welding (FSW) of CuZn40 brass alloy was performed by selecting the specified welding parameters according to the design of experiment (DOE) table. Regarding to the response surface method (RSM) with central composite design (CCD), an optimization was done according to the results of the specimen tensile test and the final function related to it was extracted. In order to achieve a predictive finite element model, an attempt was first made to consider all simulation cases regarding the experimental test. Then, by calibrating the model, while placing the optimal parameters in it, the temperature results were compared in practical mode and simulation. Finally, the relationship between welding parameters and ultimate tensile strength was investigated.

KEYWORDS Friction stir welding, CuZn40 brass alloy, Temperature contour, Response surface method, Finite element analysis.

CITE Emamikhah A, Jamali A, Kazerooni A, Mehdikhani Soleimanloo A. Friction Stir Welding of CuZn40 Brass Alloy based on Optimal Response Surface Results: Numerical and Experimental Analyses. Advanced Journal of Science and Engineering. 2021;2(1):3-17.

DOI https://doi.org/10.22034/advjscieng21021003

URL https://sciengpub.com/adv-j-sci-eng/article/view/advjscieng21021003

INTRODUCTION

In friction stir welding (FSW), a welding tool with two parts namely shoulder and pin, rotates at a defined speed and at the same time feeds at a constant welding speed to the weld line between the materials being welded.[1] In order to keep the sheets during welding, they are completely clamped. In friction stir butt welding, pin length is slightly shorter than the sheet thickness and the tool shoulder have contact with the sheet surface. The process starts with plunging the tool into the workpiece.[2, 3] In contact, frictional heat is generated within the material of workpiece on one hand and pin and shoulder which are resistant to wear on the other hand, causing the stirred material to soften without going up to the melting point and a solid state joint is formed.[4, 5] Thus, linear movement of the tool becomes possible within the plasticized zone of materials.[6] Fig. 1 illustrates a schematic illustration of this process. Mechanical and microstructural properties of brass alloys are characterized by Zn content. Muntz brass (Commercial name: C 2800) is a Cu-Zn brass alloy containing up to 38-42% zinc and has a deep bronzed color that improves its decorative and architecture applications. They also are known as duplex brass due to microstructure

of alloy containing more than 38% Zn with dual phase structure of α+β. Strength of this alloy increases with higher Zn content which leads to advantageous properties such as hot formability, machinability, forgeability and wear resistance for blanking, forming, bending, shearing, upsetting, hot heading and pressing. Therefore, they are extensively applicable in architectural panels, large architectural trim, sheet, door frames, decoration, pipe fittings, domestic taps, gas appliances and heat exchangers. High zinc content also makes the cost lower economically.[7-9]

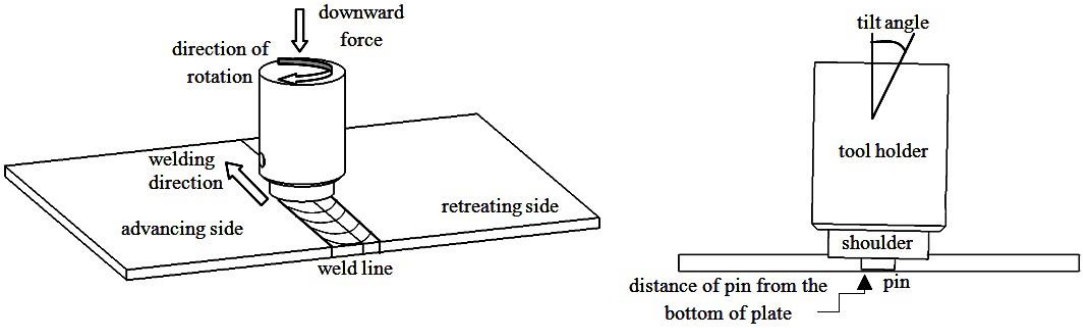

Fig. 1: Schematic of friction stir welding process.

With regard to aforementioned applications, welding is an inevitable technique for manufacturing and joining of these alloys. However, high temperatures applied in fusion welding methods contributes to dezincification and creation of fumes due to difference between the melting point of copper and zinc.[10, 11] Hence, the loss of zinc content changes the phase structure of dual phase brass alloys.[12] In FSW, for its solid-state nature, welding is carried out below the solidus temperature. Ramesh et al. showed weld zone of dual phase brass is preserved by retention of zinc during FSW process. Increasing rotational speed modified the microstructure to finer grains by dynamic recrystallization and a reduction in inhomogeneous recrystallization was observed.[13] Meran reported suit stirring of materials in FSW of CuZn30, makes no pore and evaporation. Also, using suitable welding parameters, the tensile strength of the weld metal and the base metal converge.[14]

FSW of brass alloys has been reviewed by researchers to scrutinize the effects of welding process parameters and output results like temperature, residual stresses, and microstructural evolutions. Zhao et al. investigated outcome of rotational speed on the weld properties of 2-mm-thick dissimilar CuZn40 brass/copper metals.[15] Cam et al. showed FSW can properly produce defect-free butt joints on 3-mm-thick 63% Cu-37% Zn brass sheet.[16] Cam et al. also indicated that sound FSW brass joints are obtained in a combination of selecting rotational and welding speeds.[17] Esmaeili et al. assessed the microstructure of aluminum 1050 to CuZn30 brass and indicated better FSW joints are formed as a result of higher material stirring.[18] Moghaddam et al. focused on the formation of stir bands as a strengthening structure during FSW of 5-mm thick CuZn30 brass alloy and the role of welding speed on the density of these bands.[19] Xu et al. employed FSW rapid cooling to weld 2-mm-thick 70/30 brass alloy and reported no micropores in the stir zone and no obvious HAZ as a result of post-annealing effect.[20] Sun et al. indicated higher tensile properties through FSW of Cu-30Zn alloy, indicative of enhanced materials stirring in the stir zone.[21] A notable grain refinement because of discontinuous recrystallization and subsequent strengthening were observed by FSW of Cu-30Zn brass in the survey of Mironov et al.[22]

Applying numerical, analytical and mathematical calculations unveil extensive knowledge over complex thermomechanical conditions in FSW process. Many researches have been done in thermomechanical processes employing these calculations for total life-time costs reduction, measuring uncontrollable parameters, promoting engineering science and estimation of material flow and behavior. Shojaeefard et al. employed Taguchi optimization technique in 2.5-mm-thick dissimilar aluminum to brass Friction Stir Lap Welding (FSLW) and reported rotational speed as a most effective factor in the joint tensile strength.[23] In another study, Shojaeefard et al. in FSW of AA1100 aluminum alloy used Taguchi optimization method on the platform of microstructural simulation and mechanical tests and addressed welding speed as a significant factor influencing grain size of the weld.[24] Safeen et al. successfully carried out response surface methodology (RSM) with central composite design (CCD) to estimate the mechanical properties of FS-welded AA6061-T6.[25] They showed that tool geometry is an effective factor in determining the mechanical properties. Ghaffarpour et al. used RSM to optimize FSW parameters of dissimilar 6061 and 5083 aluminum alloys to check the tensile strength.[26] Farzadi et al. further used RSM to observe a large window

of weld parameters and their interactions on the UTS of AA7075-T6 aluminum alloy, manufactured through FSW.[27] Heidarzadeh optimized the FSW parameters by RSM and comprehensively studied the microstructure of 2-mm-thick 70/30 brass joints.[28] Heidarzadeh then reported rotational speed and axial force as the effective weld factors on the joint UTS and elongation. Hence, optimization of FSW parameters considering tensile strength as an objective function have been numerously studied.[29-31] Besides, the numerical studies of FSW process have been extensively accompanied by different scientific works.[32]

Considering introductory literatures, some limited researches have been performed on the FSW of dual phase brass. A field survey showed that there was not complete knowledge on the thermal modeling of this alloy. In this study, calculated statistical values parameters and their interactions were obtained by response surface method (RSM) as a mathematical model in a range of welding parameters to evaluate the weld characteristics. Then, an exact 3D symmetrical modeling based on the experiment was done using ABAQUS software linking with FORTRAN and DFLUX subroutine with GOLDAK equations to scrutinize the thermal conditions. Then the effect of FSW process on the FS weld properties was investigated through related tests. The combination method discussed in this article is a way to determine the complexities engaged during thermomechanical processes and can be contributed as an algorithm to the similar manufacturing processes.

MATERIALS & METHODS

Experimental Investigation

For the experiments, CuZn40 brass sheets with dimensions of 100×70×3 mm^3 were prepared using grinding and cutting. These sheets are produced by cold rolling. The chemical content and mechanical properties of the welded metal are accordingly shown in Tables 1 and 2. Prior to the welding, a preheating was applied to the sheets at a temperature of about 57-60 °C.

Table 1: Chemical content of the welded metal (mass %).

Material	Sn	Fe	Ni	Zn	Cu
CuZn40	≤ 0.3	≤ 0.05	≤ 0.3	Rest	59

Table 2: Mechanical properties of the welded metal.

Material	Yield strength (Mpa)	Tensile Strength (Mpa)	Elongation (%)	Density (g/cm^3)	Shear strength (Mpa)
CuZn40	< 200	300-420	<55	8.41	235

A converted Siemens FSW machine with 5 kW power of electromotor equipped to an inverter for changing the frequencies to various rotational and travel speeds was used considering manufacturing limitations, total life-time costs and welded materials.[33] Welding was performed in butt configuration and surfaces were cleaned off precisely. By virtue of high forces and pressures arising in FSW process and high thermal diffusivity of brass alloys which are several times more than nickel alloys,[10] the sheets were clamped in a fixture. Moreover, for better temperature measurement, three thermocouples (type K) were embedded in the fixture body just 0.5 mm beneath the below parts of the sheet and in the weld line boundary (border of tool motion). The thermocouples 1, 2, and 3 were kept constant from the weld starting point in distances of 35, 50, and 65 mm respectively. The temperature contours were obtained by connection of these thermocouples to a main thermometer (type Lutron TM-947SD and temperature range -100 to 1300 °C) and a data acquisition system (DAQ).

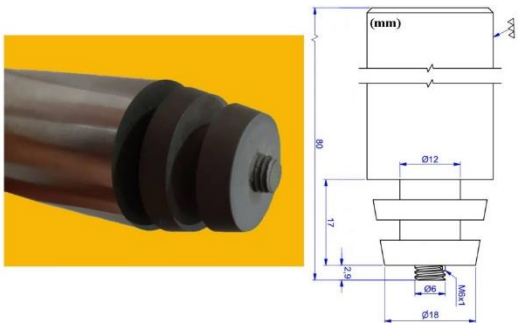

Fig. 2: Dimensions of welding tool.

The effect of FSW tool as a main parameter is studied in different investigations.[34, 35] Respecting earlier experience,[36] in this experiment, a threaded cylindrical tool pin profile made of X40CrMoV5-1 tool steel alloy (DIN 1.2344) is accurately machined. Then, to endure high pressure and temperature aroused meanwhile the welding, hardened about 60 HRC, and reached the last tolerance size. Fig. 2 shows the geometry and dimensions of this tool.

Fig. 3: Crown side of the FSW No. 4.

After welding with regard to FSW parameters presented in Table 4, specimens were labeled separately. All welds were visually inspected. Thus, specimens were approved for next tensile test. Fig. 3 indicates a labeled FSW weld (No. 4). Thereafter, three tensile test samples were cut through the welded specimens conforming to ASTM-E8.[37] After preparation, samples were transversely drawn at a continuous speed of 5 mm/min by Zwick/Roell Z100 testing machine. To evaluate the weld microstructure via optical microscopy, a sample of joint number 6 was separated and etched using a Poulton's reagent for 20 s after polishing. SEM and EDS tests were also applied to scrutinize the stir zone. KOOPA-UV1 hardness testing machine was employed to measure the Vickers micro-hardness of four samples with the highest strength according to the ASTM E-18 standard. First, the samples were prepared with dimensions of 30×10 mm^2. Then, hardness distribution of the weld was obtained by applying a force of 20 g for a time of 10 s.

For optimization, obtained results of ultimate tensile strength (UTS) tests were introduced as an objective function (output variable) into Design-Expert software (version 9.0). Then, using ANOVA (analysis of variance) table, the results were studied and conforming to available data, the accuracy of the model was confirmed. In addition, three samples were accomplished, and average of them was recorded as an output response.

Table 3: Values and levels of FSW parameters.

Parameters/Levels	Symbol	Level (-1)	Level (0)	Level (+1)
Rotational Speed (RPM)	A	900	1050	1200
welding Speed (mm/min)	B	25	50	75
Tool Tilt Angle (Degree)	C	2	2.5	3

Table 4: DOE results.

No.	Run	Welding Speed (mm/min)	Rotational Speed (RPM)	Tool Tilt Angle (Degree)	Ultimate Tensile Strength (MPa)	Fracture Location
1	15	75 (0)	1200 (-1)	2 (0)	316.75	Base metal
2	14	25 (0)	1200 (+1)	3 (0)	323.68	Base metal
3	7	75 (-1)	900 (+1)	3 (+1)	316	Weld metal
4	6	25 (-1)	900 (-1)	2 (-1)	292.63	Weld metal
5	5	50 (-1)	900 (0)	2.5 (0)	313.96	Base metal
6	9	50 (0)	1200 (0)	2.5 (-1)	326.61	Base metal
7	12	25 (+1)	1050 (0)	2.5 (0)	261.78	Weld metal
8	4	75 (+1)	1050 (-1)	2.5 (+1)	326.58	Base metal
9	8	50 (+1)	1050 (+1)	2 (-1)	289.65	Weld metal
10	13	50 (0)	1050 (0)	3 (+1)	296	Weld metal
11	2	50 (0)	1050 (0)	2.5 (0)	299.8	Weld metal
12	3	50 (0)	1050 (0)	2.5 (0)	300.2	Weld metal
13	11	50 (0)	1050 (0)	2.5 (0)	305.3	Base metal
14	10	50 (0)	1050 (0)	2.5 (0)	299.85	Weld metal
15	1	50 (0)	1050 (0)	2.5 (0)	300.1	Base metal

For design of experiment (DOE), composite central design (CCD) quadratic model applicable in response surface method (RSM) with three levels (+1, 0, -1) and five center points was used according to Table 3. The max level (+1) and min level (-1) belong to the value of the FSW parameters. Also, the value of α is considered 1. Since, rotational speed, welding speed, and tool tilt angle are controllable parameters by FSW machine, proper selecting of these parameters causes better stirring and favorable welds consequently. Thus, these parameters named as rotational speed (A), welding speed (B), and tool tilt angle (C) accordingly. The outcome of FSW tool has thoroughly discussed elsewhere.[36] Through the design experiment, 15 experiments achieved and welding was done according to them. In Table 4, the UTS of each run and corresponding levels as well as fracture location of each specimen are presented.

Simulation of FSW Process

Abaqus 6.17 software and FORTRAN codes were developed to simulate the process. FSW is a thermo-mechanical process, but thermo-mechanical welding simulation using the proposed CEL (Coupled Eulerian-Lagrangian) and ALE (Arbitrary Lagrangian-Eulerian) methods requires powerful computers and higher costs. For simulation, a thermal model was evolved and acceptable results were achieved. Other information is also coded to the software to speed up the process analysis. Simulation prerequisites like dimensions of the tool and workpiece, mandatory constraints, backing plate, and primary welding conditions were precisely introduced in agreement with the experiment. The sheet was modeled as solid deformable and then necessary partitions were applied. To increase the model validity and due to higher temperatures during the welding, properties were defined as temperature-dependent. Hence, in the property module a temperature-dependent solid homogeneous section was assigned to the sheet. The physical properties of CuZn40 brass alloy are given in Tables 5, 6, and 7, respectively.[38] In this module, the conductivity of the steel backing plate was also applied according to Table 8.

Table 5: Conductivity of CuZn40.

Conductivity (W/m.K)	Temperature (K)
0.1251	325.65
0.1368	405.35
0.1423	456.25
0.1485	511.65
0.141	1172.85
0.072	1177.85

Table 6: Density of CuZn40.

Density (kg/mm^3)	Temperature (K)
0.00839	293
0.00789	1173
0.0072	1178
0.00687	1373

Table 7: Specific heat of CuZn40.

Specific heat (J/kg.K)	Temperature (K)
390	300.85
440	700.85
480	1173.85
490	1178.85

Table 8: Conductivity of backing plate.

Conductivity (W/m.K)	Temperature (K)
0.0238518	302
0.0236639	482
0.0247659	722
0.0268122	1022
0.0288851	1262

Conforming to the experiment, time period for weld pass was considered 240 s and a heat transfer solver was defined in the step module to converge the problem. The sink temperature was regarded as 25 °C and the temperature-dependent heat transfer coefficient was given by eq. (1).[39]

$$h = \begin{cases} 0.0668\,T \ \ \left(\frac{W}{m^2}\right) & 0 < T < 500\,^{\circ}C \\ 0.231\,T - 82.1 \ \ \left(\frac{W}{m^2}\right) & T > 500\,^{\circ}C \end{cases} \quad (1)$$

Where, T is temperature. This boundary condition was assigned to all surfaces except the lower surface which is connected to the backing plate. For this, a conductivity coefficient of 50 W/m.K was assigned to the lower surface of the sheet.[40] Although on a microscopic scale, there are some air gaps between the sheet and the backing plate. In order to simplify it, it is assumed that the two are in perfect and ideal contact with each other.

In loading environment of Abaqus, initial temperature of the sheet and a volumetric heat flux FORTRAN code was assigned to the software. For meshing procedure, 13425 hexahedron heat transfer linear type elements with thermal degree of freedom were allocated to the deformable sheet and backing plate. Regarding the importance of weld line compared to its adjacent regions, a bias meshing with ratio of 0.5 was used toward the weld line. Also, to increase the model validity, more meshes were poured through the thickness direction. Moreover, at the intersection of the tool/sheet, much smaller mesh was used. Finally, regarding the lower importance of the backing plate and only having heat transfer with the sheet and in order to help Abaqus run faster, a larger mesh was poured in the backing plate compared to the sheet. The final proposed mesh is shown in Fig. 4.

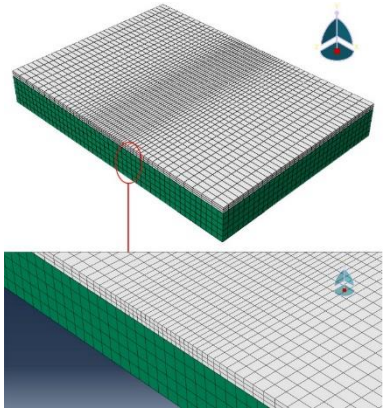

Fig. 4: Final mesh in the proposed FSW simulation.

It is obvious that alternations in elements number will influence the model results. According to Fig. 5, for mesh sensitivity, the number of elements were considered 9489, 10815, 12615, 13425, 14235, and 16395 respectively. However, there was a negligible difference between the 13425 and 12615 elements number. Thus, 12615-element was totally utilized for thermal evaluation.

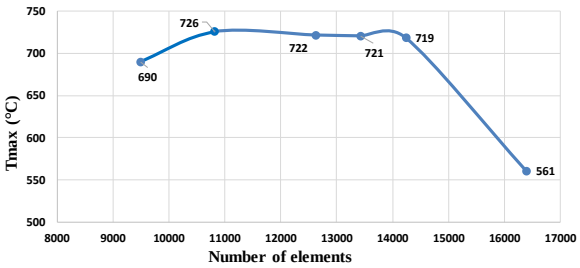

Fig. 5: Mesh sensitivity convergence test.

DFLUX Subroutine

To apply heat flux to the sheet, GOLDAK method through a DFLUX subroutine written by FORTRAN programming language was addressed to the software. GOLDAK model uses double-ellipsoidal-conical heat power density,[41] but in FSW due to axisymmetric tool and by entering the same values for width (a) and length (C_r, C_f), heat will symmetrically transfer in a shape that is almost like two hemispheres. However, considering the sheet thickness and the difference in depth (b) compared to the other two dimensions, the symmetry of volumetric heat source or two hemisphere changes. Studies show that about 85% of total generated heat in FSW is owing to the shoulder tip's surface, while this amount is 15% for the pin.[42, 43] Regarding the thermal history in FSW of brass alloy joints, elements have no mechanical degree of freedom and on the other hand, generated heat is a combination of

frictional heat and plastic work.[44] Thus, the effects of plastic deformation and inter-object friction have been considered in the thermal model. In general, source of heat generation is sliding friction between the material and tool on one hand and sticking friction due to deformation on the other hand and can be expressed as eq. (2).[45]

$$Q_{total} = \delta Q_{sticking} + (1-\delta)Q_{sliding} \quad (2)$$

According to eq. (3), δ constant is contact state variable and represents the ratio of the velocity of contact points (v_{cp}) in the tool-sheet interface with the velocity of tool point (v_{ω}) in contact.[46]

$$\delta = \frac{v_{cp}}{v_{\omega}} \quad (3)$$

To calculate the value of δ, it was calibrated by trial and error method and running 25 simulations. With regard to the contact pressure (p) originating from severe deformation and ignoring the minor heat source like pin's surface, eq. (2) will evolve into the eq. (4).[43, 46]

$$Q_{total} = \frac{1}{12}\pi\omega[(1-\delta)\mu p + \delta\tau][D^3 - d^3] \quad (4)$$

Where ω is angular rotation of the tool, μ indicates the coefficient of friction, τ is shear strength, D is shoulder diameter, and d is pin diameter.

In GOLDAK thermal model, the front and rear heat sources inside the ellipsoid are defined in eqs. (5) and (6), respectively.

$$q_r(x.y.z) = \frac{6\sqrt{3}f_r Q_{total}}{abc_r\pi\sqrt{\pi}} e^{(-3x^2/a^2)} e^{(-3y^2/b^2)} e^{(-3z^2/{c_r}^2)} \quad (5)$$

$$q_f(x.y.z) = \frac{6\sqrt{3}f_f Q_{total}}{abc_f\pi\sqrt{\pi}} e^{(-3x^2/a^2)} e^{(-3y^2/b^2)} e^{(-3z^2/{c_f}^2)} \quad (6)$$

Where x, y, and z are the coordinate axis of the workpiece; the fractions f_r and f_f determine heat deposited in front and rear regions, where $f_r + f_f = 2$. The values of f_r and f_f are equally put 1 for approaching to the experimental results. The independent parameters a, b, c are width, depth, and length of weld pool respectively and define the shape and size of moving heat source.[47] If z' in eq. (7) replaces z in eqs. (5) and (6), the heat source moves linearly in z-axis direction conforming to the velocity of the tool (v) and time (t).[46]

$$z' = z - v.t \quad (7)$$

RESULTS & DISCUSSION

Numerical Analysis

The accuracy of developed model was estimated by analysis of variance (ANOVA). The ANOVA results for UTS are presented in Table 9. Referring to the Table 9, the predicted regression conforming to ANOVA results has 9 degree of freedom (DOF) which three of them belong to the main parameters (linear effects), other three ones are pertaining to the square of main parameters and the rest are belong to the interaction effects of two main parameters. Whenever the P-value of the model is below the allowable error level (0.05 in this model), the effect of model terms on the response is statistically significant. In this model, the P-value is 0.0002. According to ANOVA table, rotational and welding speed have the P-value lower than 0.05, but this value for tilt angle is greater than 0.05. Thus, notwithstanding the tilt angle, the effect of two other parameters is significant. Besides, F-value shows the adequacy and reliability of model without random data and noise determining the effect of each parameter on the response.[48] The higher the F-value, the greater effect the parameter. Therefore, an increase in F-value will influence the relevant response of that parameter. F-value of 52.7 shows the accuracy of the model. Amongst the process parameters of this analysis, welding speed between the interactions, rotational speed-tilt angle with values of 248.05 and 126.08 respectively, have the most effect on the ultimate tensile strength (UTS). Totally, the effects of A, AB, AC, and A^2 terms are significant. It is noted that the value of R^2 is 0.9896 which illustrates the accuracy of model prediction. Also, the values of Adj R-Squared and Pred R-Squared must be near not more than 0.2.

Table 9: ANOVA table.

Source	Sum of Squares	DOF	Mean Square	F-value	P-value
Model	4014.48	9	446.05	52.70	0.0002
A-Rotational Speed	80.01	1	80.01	9.45	0.0276
B-Welding Speed	2099.52	1	2099.52	248.05	<0.0001
C-Tool Tilt Angle	20.16	1	20.16	2.38	0.1834
AB	25.81	1	25.81	3.05	0.1412
AC	1067.10	1	1067.10	126.08	<0.0001
BC	3.52	1	3.52	0.42	0.5474
A^2	1235.20	1	1235.20	145.94	<0.0001
B^2	50.01	1	50.01	5.91	0.0593
C^2	85.81	1	85.81	10.14	0.244
Residual	42.32	5	8.46	Adeq Precision	27.2920
Std. Dev.	2.9093	R-Squared (R^2)	0.9896	Adj R-Squared	0.9708
Mean	304.5927	C.V. %	0.9551	Pred R-Squared	-0.0954

The UTS value predictor function expressed in eq. (8).

$$UTS = 299.94 + 6.33 \times A + 32.40 \times B + 3.18 \times C - 4.40 \times AB + 28.29 \times AC - 1.62 \times BC + 21.73 \times A^2 - 4.37 \times B^2 - 5.73 \times C^2 \quad (8)$$

The normal plot of residuals of the UTS indicates the correct distribution of errors. Fig. 6 shows the graph of predicted against actual values. More proximity of the corresponding points to the trend line illustrated the higher accuracy of the model and a suitable concurrence between the predicted and actual values.

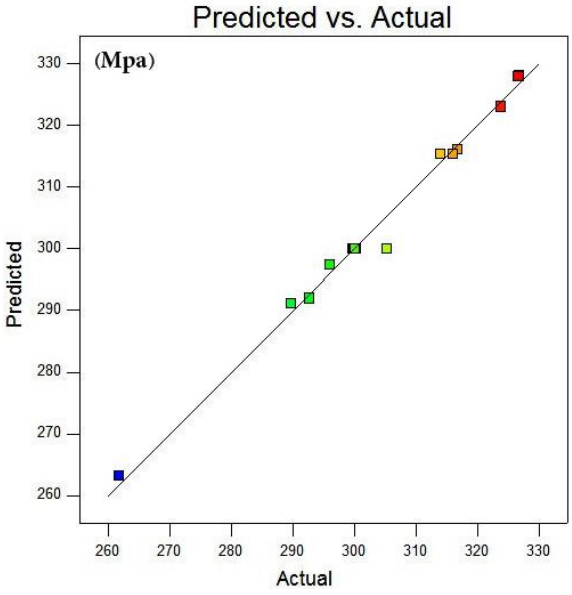

Fig. 6: Predicted against actual values for ultimate tensile strength.

Optimization is dependent on the requested target. There are three modes for optimization. In the first case, the answers are in a specific range, which is known as the target range. In the second case, optimization means putting the answer in its highest value, and finally in the third case, optimization is to get the answer in the least possible amount.[48] Here, the answer is that the UTS of the welded specimens should be maximized to be optimal. Respecting the DOE results in Table 4, the maximum and minimum values of UTS (326.61 and 261.78 MPa in the joint numbers 6 and 7, respectively) were introduced as input parameters to the RSM model. Also, the value of desirability was regarded 1. For confirming the predicted model, the parameters of the joint number 6 with maximum value of UTS was compared to the experiment and the percentage of error was 0.42 according to table 10. This shows the accuracy of the model in response evaluation.

Table 10: Predicted RSM model for the joint number 6.

A	B	C	UTS	Desirability
1200 RPM	50 mm/min	2.5	327.997	1

With regard to some limitations in Abaqus software to move volumetric heat source, DFLUX subroutine was employed. All equations and mathematical statements, GOLDAK variables, welding parameters, and necessary constants was codified in FORTRAN language and was linked to Abaqus to run the heat source according to the optimal values parameters confirmed by RSM method. These values are shown in Table 11. Also, Fig. 7 indicates the variations in the volumetric heat source for FSW process.

Table 11: DFLUX subroutine variables.

Variable	Value	Variable	Value
a (mm)	9	F (KN)	40
b (mm)	2.8	Rotational speed (RPM)	1200
C_r, C_f (mm)	9	Welding speed (mm/min)	50
τ (MPa)	235	Shoulder diameter (mm)	18
Sink temperature (°C)	25	Pin diameter (mm)	6
δ	0.054	μ	0.5

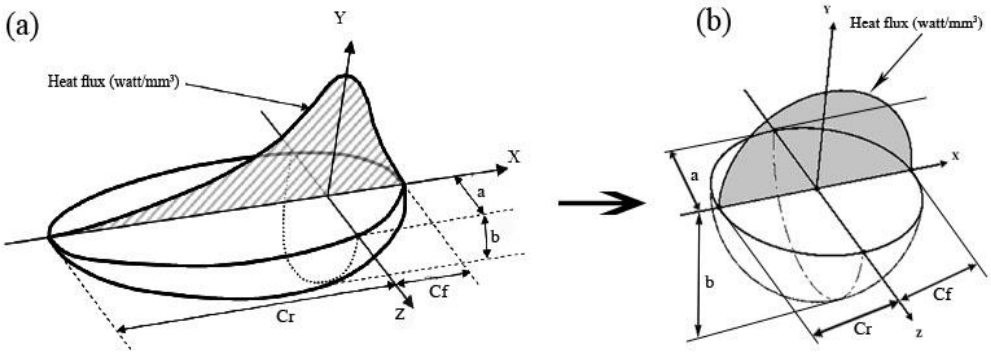

Fig. 7: a) Heat source of GOLDAK model, b) The FSW heat source.

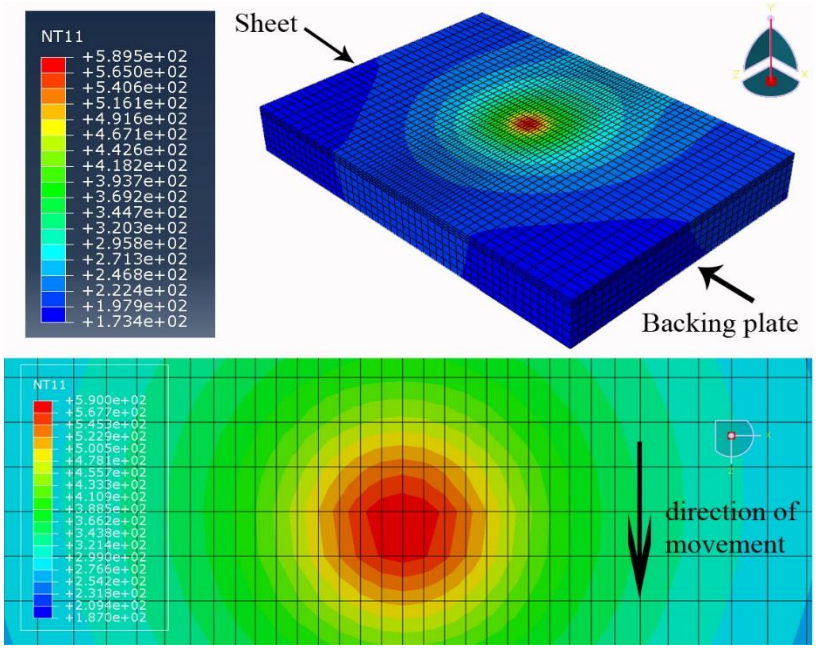

Fig. 8: Temperature distribution analysis and the shape of heat transfer pool at the end of the simulation.

Fig. 8 shows the temperature distribution in the simulation in the 115th second. According to the results, with the passage of time and the heat source crossing in the weld line, the temperature distribution also changes homogeneously, and the maximum temperature occurs near the heat source. As can be seen from the Fig. 8, unlike the fusion welding, in which the shape of the weld pool consists of double-ellipsoid, in FSW, the shape of the heat source is almost like a sphere due to the symmetrical conditions of heat applied by the shoulder.[49] In the simulation results, it was observed that as the tool moves toward the end of the sheet, the leading side of the shoulder, which forms the front zone of the heat transfer pool, generates a little more heat than the trailing side and its symmetrical shape tends to be elongated.[50]

Fig. 9 shows the combined temperature diagrams obtained from both the experiment and simulation. Comparing the thermal results, an acceptable correlation between the simulation and experiment is observed. However, some minor differences can occur for a variety of reasons, such as not considering the radiant heat transfer and ignoring the surface temperature of the pin's surface in the calculations which was mentioned earlier. Therefore, the model presented along with DFLUX subroutine and GOLDAK equations can be employed without tool and with the help of the subroutine to investigate the changes of solid state welds. Therefore, with the correct definition of FSW welding in this model, it is possible to investigate the desired outputs according to the operating parameters of the process.

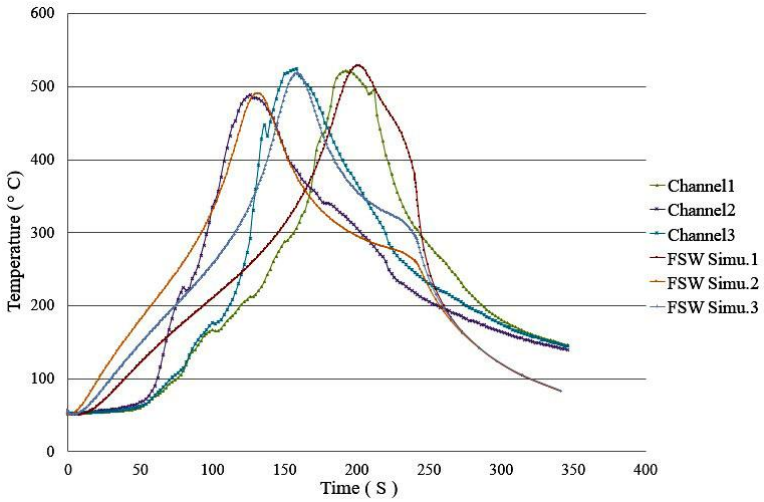

Fig. 9: The temperature diagram extracted after simulation and experiment.

The relationship between inputs and outputs parameters was evaluated by the RSM model in two and three dimensional spaces. To investigate the effect of the two parameters on each other, the third one was kept constant at its zero level to the extent that by changing it, the model can be investigated. Fig. 10 illustrates the effects of varying rotational speed and welding speed on the UTS. As the rotational and welding speeds becomes more, so does the UTS. Also, when the rotational speed of the tool approaches to the zero level (1050 RPM), to achieve the higher UTS, the tool's welding speed must be selected at the highest level. The reason for this is more heat generated, which was confirmed by measuring the temperature in the experiment and simulation. It should be noted that microstructural evolutions are also a reason for increasing UTS.[51, 52] Based on the results of tensile test and temperature measurements, it was found that the highest temperature is obtained by rising the rotational speed and decreasing the welding speed. In joint number 2, with the most rotational speed and the lowest welding speed of 1200 RPM and 25 mm/min, the highest temperature was measured as 524.7 °C compared to other joints.

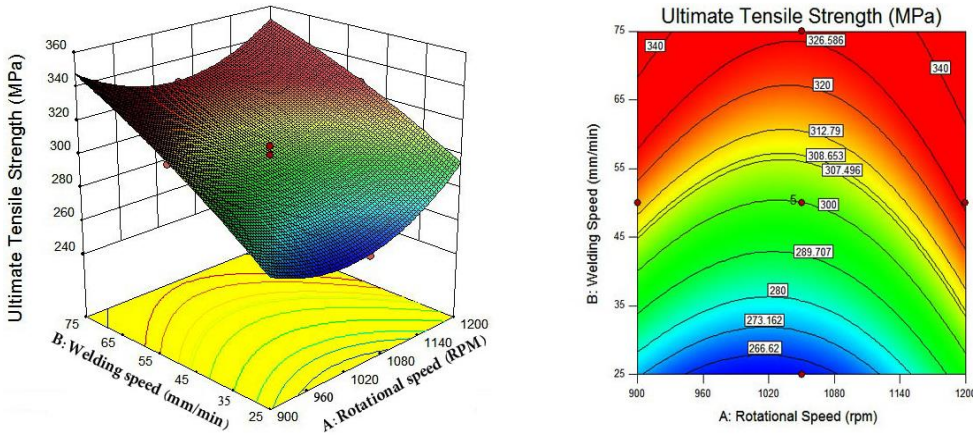

Fig. 10: Interactions of rotational and welding speeds on the UTS.

Fig. 11 illustrates the interactions of welding speed and tilt angle on the UTS. As presented, the UTS of the welded specimens increases with increasing welding speed. The maximum UTS was measured in joint number 6, equal to 326.61 MPa, where the rotational speed, welding speed, and tilt angle were adjusted at 1200 RPM, 50 mm/min and 2.5°, respectively. It should be noted that the maximum temperature in this joint was recorded at 504 °C.

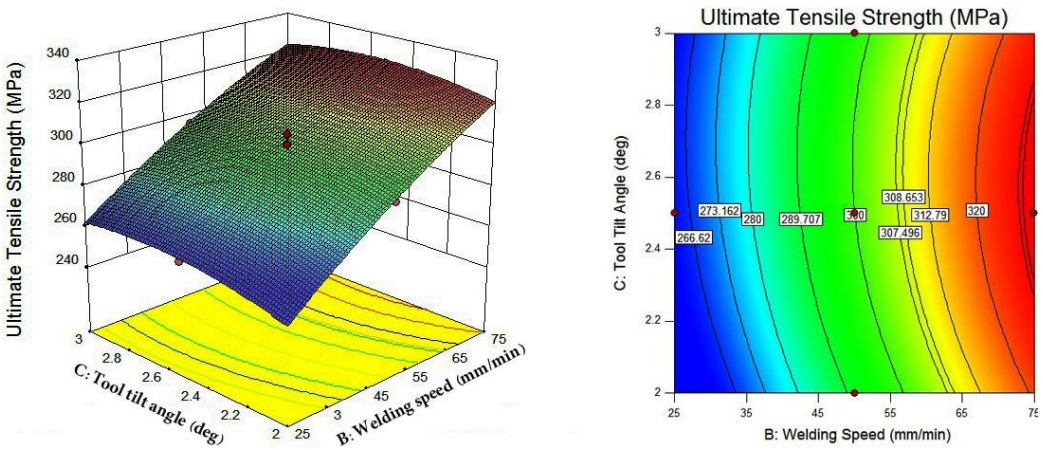

Fig. 11: Interactions of welding speed and tool tilt angle on the UTS.

Experimental Analysis

Materials stirring below the FSW tool due to gradient in the temperature, strain rate and strain, results in a remarkably distinctive microstructure, which can be separated into four regions, namely stir zone (SZ), thermo-mechanically affected zone (TMAZ), heat-affected zone (HAZ) and base metal (BM) [51]. Since the highest amount of UTS was measured in the joint number 6, a microstructural evaluation of this sample was investigated to understand the weld properties. According to Fig. 12, the grain size has altered significantly toward the weld zone, to the extent that there is more grain refining in the stir zone. Actually, rotation of the tool causes stirring of the material below the tool shoulder and leads to the microstructural evolutions. Additionally, this stirring, as well as the heat generated, induces the materials to become fine.

In the TMAZ region, the effects of high temperature and strain rate are lower than in the SZ region (Fig. 12). This region, which is partly affected by heat and mechanical work, has elongated grains. High-zinc brass composes two phases: α that is the predominant in the sample and β which directly results in better hot-formability of the brass alloy.[7] According to the microstructural developments presented in the Fig. 12, the grains undergo severe plastic deformation and new grains are formed due to recrystallization and regarding high numbers of nucleation the refinement occurs. Also, SEM and EDS studies showed no trace of zinc evaporation in the stir zone (Fig. 13).

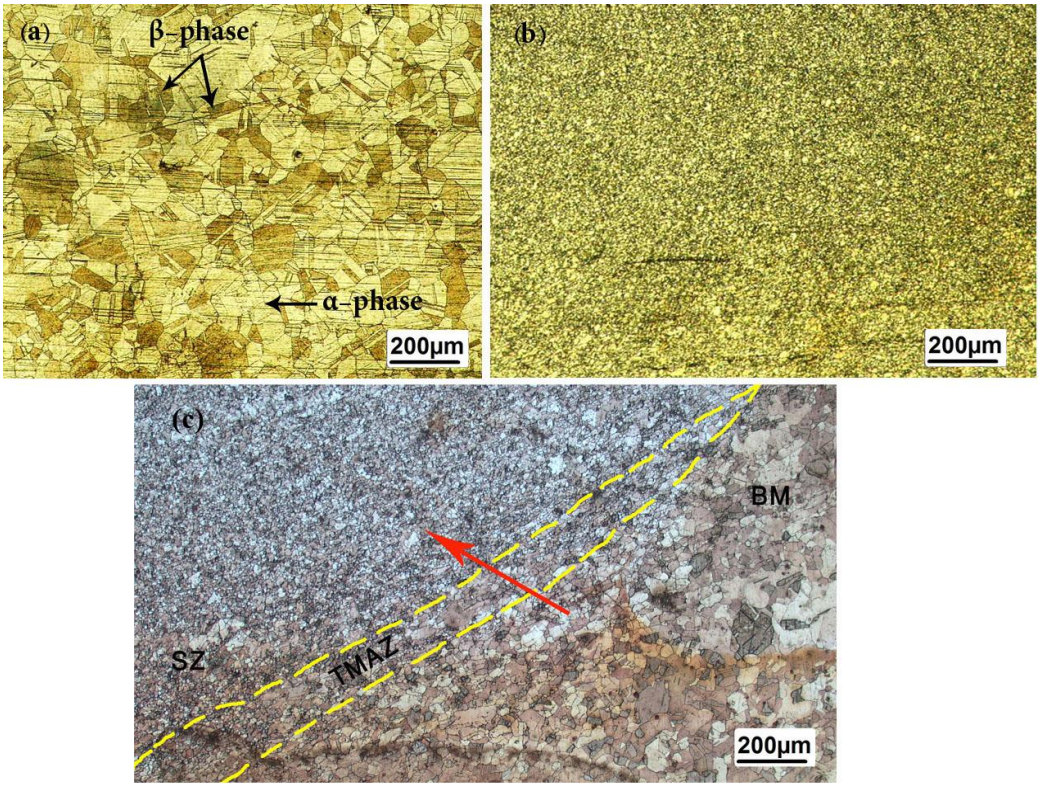

Fig. 12: a) *α* and *β* phases in CuZn40 brass alloy content, b) Effect of FSW process on phase fragmentation, c) Microstructural changes toward the weld zone.

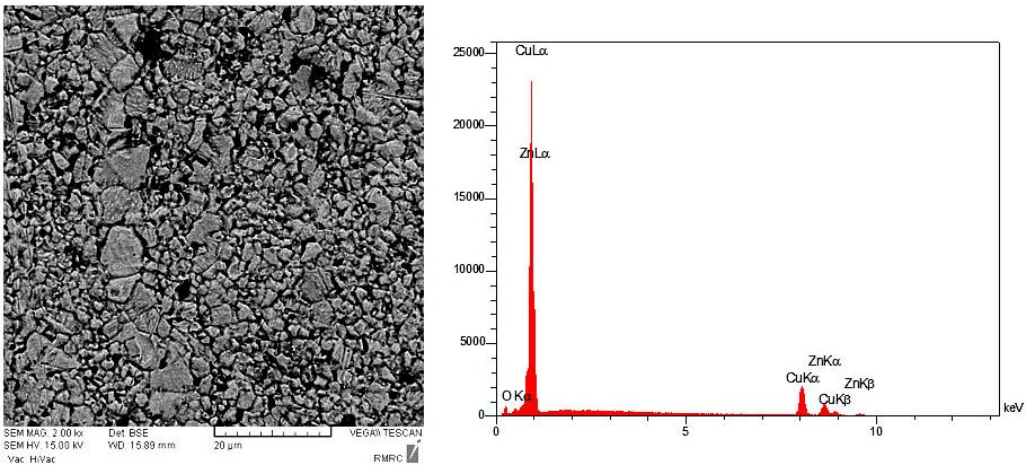

Fig. 13: Investigation of stir zone with SEM and EDS analyzes.

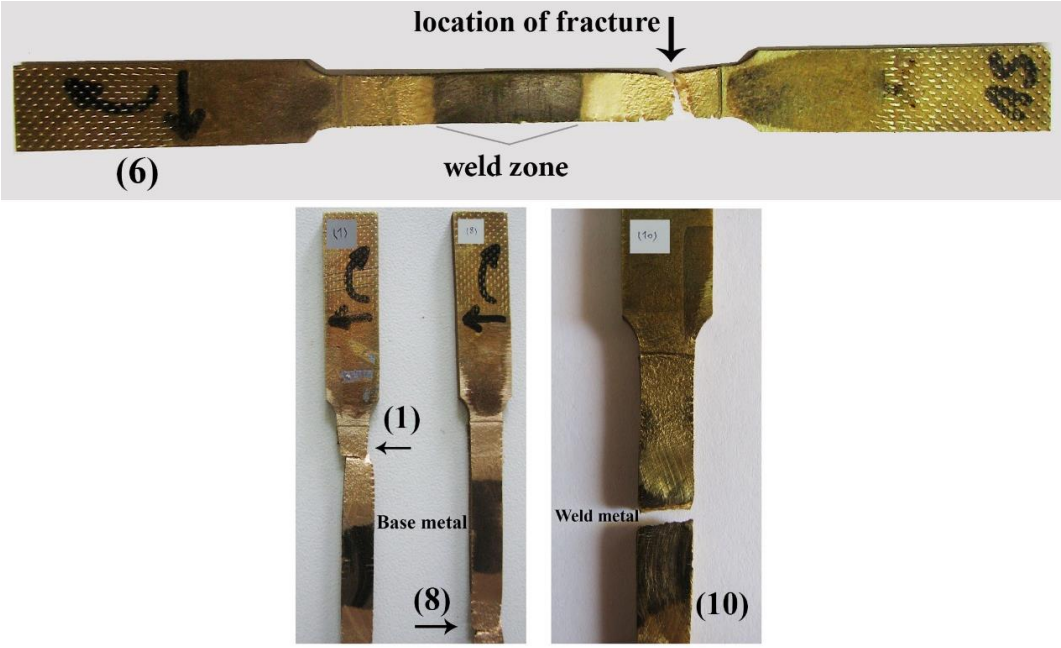

Fig. 14: The location of fracture in selected samples.

The strength of the weld metal is an important criterion in the study of the mechanical properties. Also, the microstructure of the weld metal directly affects its mechanical properties and plays an important role in the quality of the weld. The location of fracture in selected samples is shown in Fig. 14. As can be seen, the fracture point of this sample is outside the weld zone and on the base metal. This has been proven in Hall-Petch correlation of eq. (9), where the strength (σ) increases with decreasing grain size (d).[53]

$$\sigma = \sigma_0 + k_y d^{-\frac{1}{2}} \tag{9}$$

This equation is also reformulated based on the hardness (H_v) through eq. (10).

$$H_v = H_0 + k_H d^{-\frac{1}{2}} \tag{10}$$

Where k_y, k_H, and H_0 are the appropriate constants associated with strength and hardness measurements. Fig. 15 shows the micro-hardness profile of some samples toward the weld zone. The maximum hardness was in joint number 8 equal to 125.3 HV. In this sample, the maximum temperature in the advancing side (AS) of the weld was measured 499.2 °C, which rotational and welding speeds were 1050 RPM and 75 mm/min, respectively. The amount of hardness in the advancing side (AS) of the weld is higher and according to the measurements obtained from the welding temperature; the temperature in the advancing side of each weld is also higher. This shows that hardness values are also affected by temperature changes during welding due to changes in the main welding parameters.

According to the Hall-Petch correlation, eq. (10), and microstructural evolutions, it is observed that grain refining and homogeneity in stir zone are other reasons for increasing hardness. In sample No. 10, due to the grain refinement, the hardness of the weld metal is increased, but sometimes the presence of defects and impurities in the base metal or the weld weakens the tensile strength. For this purpose and to check the defect, sample No. 10 was subjected to microstructure testing using optical microscopy. However, sometimes too much localized heating applied to the stir zone causes a defect in the weld, as shown in Figure 16. This defect affects the weld strength results in the tensile test.

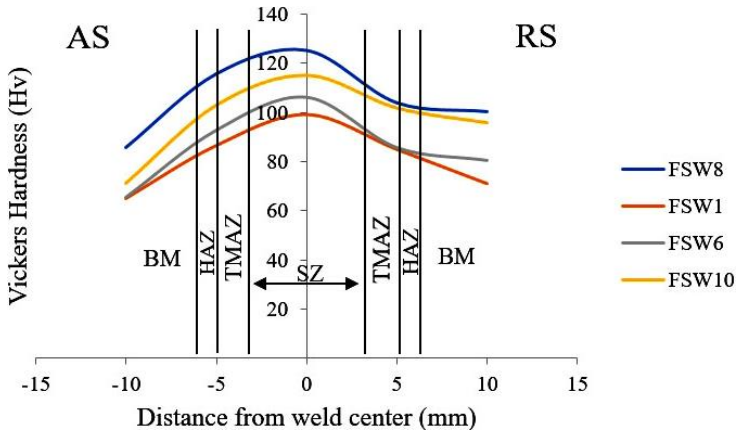

Fig. 15: Microhardness results through the cross section of the weld.

Fig. 16: Defect formation in sample No. 10.

CONCLUSION

Friction stir welding of CuZn40 brass alloy was performed well in a certain range of selected welding parameters. The optimal values obtained from the response surface method (RSM) were validated to be used in the thermal model of this process. The most important results of this research are included here. First, the ultimate tensile strength equation was extracted after optimization based on the parameters considered in the RSM. The results indicated that the effect of two parameters of rotational and welding speeds is more meaningful than tool tilt angle on the UTS of brass joints. Second, a 3D FEM thermal model of the effect of the FSW process on the CuZn40 brass alloy was simulated according to the optimal values, in which coded subroutine were used to apply volumetric heat flux. Proper matching between temperature measurement in practical mode and simulation indicates the validity of the computational model. Third, maximum amount of UTS was obtained in joint number 6 in which the rotational speed, welding speed and tool tilt angle were adjusted to 1200 RPM, 50 mm/min and 2.5°, respectively. Simultaneous mechanical work and generated heat increased mechanical properties due to the grain refinement of the material in the stir zone. Fourth, microstructural study of the stir zone showed no trace of zinc evaporation in the stir zone. Moreover, regarding the recrystallization and high nucleation rate, there is more evidence of grain refinement toward the stir zone. Fifth, the results confirmed that the hardness distribution from the base metal to the stir zone gradually increases. However, the formation of defects in the weld metal can cause a reduction in hardness in some places.

DISCLOSURE STATEMENT

The author(s) did not report any potential conflict of interest.

REFERENCES

1. Dabeer P, Shinde G. Perspective of friction stir welding tools. Materials Today: Proceedings. 2018;5:13166-13176.
2. Mandal S, Rice J, Elmustafa AA. Experimental and numerical investigation of the plunge stage in friction stir welding. Journal of Materials Processing Technology. 2008;203:411-419.
3. Shi L, Wu CS. Transient model of heat transfer and material flow at different stages of friction stir welding process. Journal of Manufacturing Processes. 2017;25:323-339.
4. Ghetiya ND, Patel KM, Patel AB. Prediction of temperature at weldline in air and immersed friction stir welding and its experimental validation. The International Journal of Advanced Manufacturing Technology. 2015;79:1239-1246.
5. He X, Gu F, Ball A. A review of numerical analysis of friction stir welding. Progress in Materials Science. 2014;65:1-66.
6. Nandan R, DebRoy T, Bhadeshia HK. Recent advances in friction-stir welding–process, weldment structure and properties. Progress in materials science. 2008 Aug 1;53:980-1023.
7. ASM. Properties and selection: nonferrous alloys and special-purpose materials. ASM: Cleveland, 1990
8. Farabi E, Zarei-Hanzaki A, Abedi HR. High temperature formability prediction of dual phase brass using phenomenological and physical constitutive models. Journal of Materials Engineering andPperformance. 2015;24:209-220.
9. Balík J, Faltus J, Janeček M. High temperature creep of modified α+ β brasses. Materials Science and Engineering A. 2008;494:113-121.
10. ASM. Welding, brazing, and soldering. ASM: Cleveland, 1993.
11. Hasan A. Studying the corrosion of brass weldments by weight losses method. Australian Journal of Basic and Applied Sciences. 2014;8:106-112.
12. Meran C, Yuksel M, Gulsoz A, Sekercioglu T. Welding problems with thin brass plates and tungsten inert gas pulse welding. Science and Technology of Welding and Joining. 2004;9:131-137.
13. Ramesh R, Dinaharan I, Akinlabi ET, Murugan N. Microstructure and mechanical characterization of friction-stir-welded dual-phase brass. Journal of Materials Engineering and Performance. 2018 Apr;27(4):1544-54.
14. Meran C. The joint properties of brass plates by friction stir welding. Materials & Design. 2006;27:719-726.
15. Zhou L, Zhou WL, Feng JC, He WX, Huang YX, Dong SS. Effect of rotation speed on the microstructure and mechanical properties of dissimilar friction stir-welded copper/brass metals. The International Journal of Advanced Manufacturing Technology. 2016;84:1335-1343.
16. Çam G, Mistikoglu S, Pakdil M. Microstructural and mechanical characterization of friction stir butt joint welded 63% Cu-37% Zn brass plate. Welding Journal. 2009;88:225-232.
17. Çam G, Serindağ HT, Çakan A, Mistikoglu S, Yavuz H. The effect of weld parameters on friction stir welding of brass plates. Materialwissenschaft und Werkstofftechnik: Entwicklung, Fertigung, Prüfung, Eigenschaften und Anwendungen technischer Werkstoffe. 2008;39:394-399.
18. Esmaeili A, Givi MB, Rajani HZ. A metallurgical and mechanical study on dissimilar friction stir welding of aluminum 1050 to brass (CuZn30). Materials Science and Engineering A. 2011;528:7093-7102.
19. Moghaddam MS, Parvizi R, Haddad-Sabzevar M, Davoodi A. Microstructural and mechanical properties of friction stir welded Cu–30Zn brass alloy at various feed speeds: influence of stir bands. Materials & Design. 2011;32:2749-2755.
20. Xu N, Ueji R, Fujii H. Enhanced mechanical properties of 70/30 brass joint by rapid cooling friction stir welding. Materials Science and Engineering A. 2014;610:132-138.
21. Sun YF, Xu N, Fujii H. The microstructure and mechanical properties of friction stir welded Cu–30Zn brass alloys. Materials Science and Engineering A. 2014;589:228-234.
22. Mironov S, Sato YS, Kokawa H. Development of grain structure during friction stir welding of pure titanium. Acta Materialia. 2009;57:4519-4528.
23. Shojaeefard MH, Khalkhali A, Akbari M, Tahani M. Application of Taguchi optimization technique in determining aluminum to brass friction stir welding parameters. Materials & Design. 2013;52:587-592.
24. Shojaeefard MH, Akbari M, Khalkhali A, Asadi P, Parivar AH. Optimization of microstructural and mechanical properties of friction stir welding using the cellular automaton and Taguchi method. Materials & Design. 2014;64:660-666.
25. Safeen W, Hussain S, Wasim A, Jahanzaib M, Aziz H, Abdalla H. Predicting the tensile strength, impact toughness, and hardness of friction stir-welded AA6061-T6 using response surface methodology. The International Journal of Advanced Manufacturing Technology. 2016;87:1765-1781.
26. Ghaffarpour M, Dariani BM, Hossein Kokabi A, Razani NA. Friction stir welding parameters optimization of heterogeneous tailored welded blank sheets of aluminium alloys 6061 and 5083 using response surface methodology. Proceedings of the Institution of Mechanical Engineers B. 2012;226:2013-2022.
27. Farzadi A, Bahmani M, Haghshenas DF. Optimization of operational parameters in friction stir welding of AA7075-T6 aluminum alloy using response surface method. Arabian Journal for Science and Engineering. 2017;42:4905-4916.
28. Heidarzadeh A. Tensile behavior, microstructure, and substructure of the friction stir welded 70/30 brass joints: RSM, EBSD, and TEM study. Archives of Civil and Mechanical Engineering. 2019;19:137-146.
29. Panda B, Garg A, Jian Z, Heidarzadeh A, Gao L. Characterization of the tensile properties of friction stir welded aluminum alloy on joints axial force, traverse speed, and rotational speed. Frontiers of Mechanical Engineering. 2016;11:289-298.

30. Ghangas G, Singhal S. Modelling and optimization of process parameters for friction stir welding of armor alloy using RSM and GRA-PCA approach. Materials Research Express. 2018;6:1-25.
31. Heidarzadeh A, Barenji RV, Esmaily M, Ilkhichi AR. Tensile properties of friction stir welds of AA 7020 aluminum alloy. Transactions of the Indian Institute of Metals. 2015;68:757-767.
32. Uyyuru RK, Kailas SV. Numerical analysis of friction stir welding process. Journal of Materials Engineering and Performance. 2006;15:505-518.
33. Bahemmat P, Haghpanahi M, Givi MK, Seighalani KR. Study on dissimilar friction stir butt welding of AA7075-O and AA2024-T4 considering the manufacturing limitation. The International Journal of Advanced Manufacturing Technology. 2012;59:939-953.
34. Salari E, Jahazi M, Khodabandeh A, Ghasemi-Nanesa H. Influence of tool geometry and rotational speed on mechanical properties and defect formation in friction stir lap welded 5456 aluminum alloy sheets. Materials & Design. 2014;58:381-389.
35. Xu W, Liu J, Zhu H, Fu L. Influence of welding parameters and tool pin profile on microstructure and mechanical properties along the thickness in a friction stir welded aluminum alloy. Materials & Design. 2013;47:599-606.
36. Emamikhah A, Abbasi A, Atefat A, Givi MB. Effect of tool pin profile on friction stir butt welding of high-zinc brass (CuZn40). The International Journal of Advanced Manufacturing Technology. 2014;71:81-90.
37. Standard test method for tension testing of metallic materials. ASTM E 8M annual book of ASTM standards. Part 8; ASTM, 1998.
38. ProCast software. Version 2018.
39. Darvazi AR, Iranmanesh M. Thermal modeling of friction stir welding of stainless steel 304L. The International Journal of Advanced Manufacturing Technology. 2014;75:1299-1307.
40. Nandan RG, Roy GG, Lienert TJ, Debroy T. Three-dimensional heat and material flow during friction stir welding of mild steel. Acta Materialia. 2007;55:883-895.
41. Goldak J, Chakravarti A, Bibby M. A new finite element model for welding heat sources. Metallurgical Transactions B. 1984;15:299-305.
42. Schmidt H, Hattel J, Wert J. An analytical model for the heat generation in friction stir welding. Modelling and Simulation in Materials Science and Engineering. 2003;12:143-157.
43. Đurđanović MB, Mijajlović MM, Milčić DS, Stamenković DS. Heat generation during friction stir welding process. Tribology Industry. 2009;31:8-14.
44. Aval HJ, Serajzadeh S, Kokabi AH. Evolution of microstructures and mechanical properties in similar and dissimilar friction stir welding of AA5086 and AA6061. Materials Science and Engineering A. 2011;528:8071-8083.
45. Yaduwanshi DK, Bag S, Pal S. Heat transfer analyses in friction stir welding of aluminium alloy. Proceedings of the Institution of Mechanical Engineers B. 2015;229:1722-1733.
46. Ebrahimpour A, Mostafapour A, Bouzary H, Salahi S. Experimental Measurement and numerical simulation of temperature distribution and thermal history during friction stir welding of pure copper joints. Journal of Mechatronics. 2014;2:113-118.
47. Velaga SK, Ravisankar A. Finite element based parametric study on the characterization of weld process moving heat source parameters in austenitic stainless steel. International Journal of Pressure Vessels and Piping. 2017;157:63-73.
48. Montgomery DC. Design and analysis of experiments. John Wiley & Sons: 8th Ed., 2012.
49. Song M, Kovacevic R. Thermal modeling of friction stir welding in a moving coordinate system and its validation. International Journal of Machine Tools and Manufacture. 2003;43:605-615.
50. Chansoria P, Solanki P, Dasgupta MS. Parametric study of transient temperature distribution in FSW of 304L stainless steel. The International Journal of Advanced Manufacturing Technology. 2015;80:1223-1239.
51. GM X, Geng L. Effects of friction stir welding parameters on microstructures and mechanical properties of brass joints. Materials Transactions. 2008;79:1698-1701.
52. Chen J, Fujii H, Sun Y, Morisada Y, Kondoh K, Hashimoto K. Effect of grain size on the microstructure and mechanical properties of friction stir welded non-combustive magnesium alloys. Materials Science and Engineering A. 2012;549:176-184.
53. Hall EO. The Hall-Petch relationship. Proceedings of the Physical Society B. 1951;64:747-753.